Synergy of photogrammetric and ULS data for forestry application through the fusion of Bundle Adjustment and ICP algorithms

Łukasz Wilk [1], Wojciech Ostrowski [1, 2], Magdalena Pilarska-Mazurek[1]

[1] Warsaw University of Technology, Faculty of Geodesy and Cartography, Department of Photogrammetry, Remote Sensing and Spatial Information Systems, Warsaw, Poland – (lukasz.wilk, wojciech.ostrowski, magdalena.pilarska)@pw.edu.pl
[2] Jagiellonian University, Institute of Archeology, Krakow, Poland

Keywords: Bundle Adjustment, Iterative Closest Point (ICP), Unmanned Laser Scanning (ULS), Ceres Solver.

Abstract

The study explores a workflow for integrating photogrammetric image blocks with LiDAR point clouds acquired via Unmanned Laser Scanning (ULS) in forestry applications. Hybrid datasets combining UAV imagery and LiDAR data are increasingly used for 3D mapping, yet discrepancies often arise due to independent orientation processes and systematic errors. Traditional solutions rely on numerous ground control points (GCPs), which can be impractical in dense forest environments. To address this, the proposed method fuses bundle adjustment and Iterative Closest Point (ICP) algorithms in a joint optimization process, aligning multispectral images with ULS point clouds without additional observations or GCPs. The workflow includes a GPU-accelerated filtering step to extract representative canopy points, reducing computational load and improving correspondence selection. Implemented using Python and C++ extensions, the system leverages the Ceres Solver for non-linear optimization, minimizing reprojection, GNSS, IMU, and point-to-cloud errors iteratively. Tests conducted in Żednia Forest District, Poland, during leaf-on and leaf-off seasons demonstrated significant improvements in alignment accuracy: average horizontal errors decreased by over 50%, and maximum offsets were reduced by more than 1 meter. These results confirm that the proposed hybrid adjustment substantially enhances geometric consistency between photogrammetric and LiDAR datasets, offering a cost-effective solution for forestry mapping and monitoring.

1. Introduction

Complex datasets composed of coupled, complementary LiDAR point clouds and photogrammetric image blocks are currently among the standard measurements used for 3D mapping. In the context of urban modeling or surveying large areas, such data is typically collected from high (aerial) altitudes. Typical sensors used for such tasks include large- or medium-format aerial cameras and aerial laser scanners (Airborne Laser Scanning, ALS). In response to the popularity of such data, special hybrid sensors have also been developed that allow simultaneous collection during a single flight. Among the most common sensors are the Leica Country Mapper, which combines ALS technology with a wide-format camera, and the Leica City Mapper and Vexcel UltraCam Dragon, which integrate ALS with 5-directional oblique cameras.

A similar trend can also be observed at lower altitudes, where photogrammetric data is collected using unmanned aerial vehicles (UAVs) equipped with regular frame cameras, multispectral (MS) cameras, and dedicated laser scanners (Unmanned Laser Scanning, ULS). Due to their enormous potential, such combined blocks are used, among other things, for 3D city modeling, forestry or monitoring of technical infrastructure.

The condition for the joint use of these two types of data is the removal of remaining discrepancies, usually resulting from independent systematic errors and orientation processes of each sensor. In most cases, differences between datasets are eliminated by using common ground control points (GCPs). In some cases, however, using multiple GCPs may be disadvantageous or uneconomical; in such cases, a potential solution is to align both data sources in a joint adjustment process. In dense forests, the use of common GCPs is very limited (bordering on impossible). For this reason, it is necessary to use a different method that accounts for the common orientation of these two data sources via correspondences.

Hybrid orientation of LiDAR data together with image blocks is an issue discussed in the literature. Hybrid orientation methods are divided into two categories - loosely coupled and tightly coupled - depending on whether the two sensors were rigidly linked to each other during data acquisition (Cledat and Skaloud, 2020). An example of implementing such a process based on a common adjustment of ALS strips and images is described by Glira et al. (2019). It is also available in the OPALS software. A similar process in the context of UAV data is also discussed by Haala et al. (2020). However, in most cases, the methods presented in the literature are intended for use in urban areas, as they rely heavily on planar features (Zhou et al., 2021).

Although the orientation methods presented above can effectively link both types of data geometrically, applying them to a wooded area requires appropriate adaptation. Point clouds obtained using dense image matching (DIM) and ULS for forest areas differ significantly in nature. As noted, for example, by You et al. (2023), point clouds and products such as elevation models are only consistent with the upper canopy surface. Therefore, it is necessary to modify the method for selecting correspondences between tiepoints and points in the ULS point cloud.

The research presented in this article addresses the issue of UAV imagery orientation with respect to ULS data in densely forested areas. The scientific contribution here lies in the methodology for accurately identifying correspondences between dense ULS point clouds and tiepoints from UAV imagery, and the subsequent registration of these two datasets. To identify tie observations between datasets, an algorithm based on iterative triangulated irregular network (TIN) densification was developed, allowing filtering of ULS points located on the canopy surface. In the next step, an algorithm

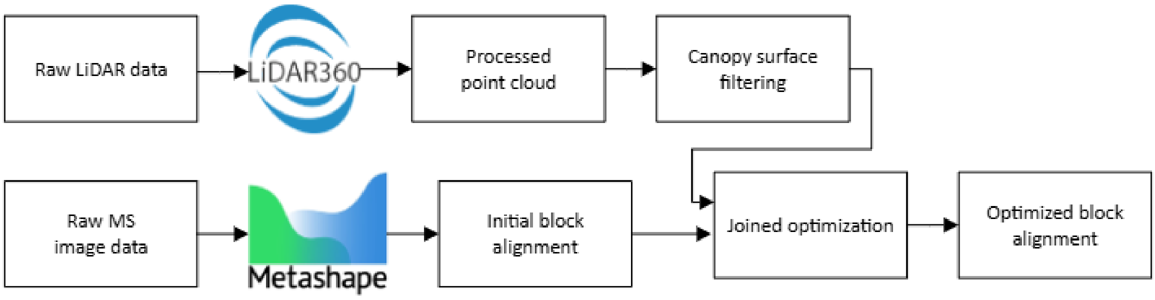

Figure 1. An overview of the processing workflow for MS and ULS data in the hybrid adjustment process.

was implemented that combines bundle adjustment and the Iterative Closest Point (ICP) algorithms, which, based on filtered point clouds from ULS, performs image block orientation to minimize the discrepancy between image and LiDAR data while maintaining the internal geometric consistency of the image block and the absolute position dictated by measurement data from the GNSS system.

2. Method and software

Since the implemented orientation process uses the ICP method, it is necessary to filter the ULS point cloud prior to processing (Figure 1). The tree filtering process plays two important roles. Firstly, to fractionate the input point cloud used as a reference in the ICP process. A smaller point cloud reduces memory consumption and speeds up calculations. Secondly, the algorithm selects only points that can be captured in both the ULS point cloud and the tiepoint cloud generated by UAV image matching. In dense forests, only representative points on the canopy surface need to be selected.

This issue is often discussed in the context of building a canopy height model (CHM), where it is necessary to eliminate within-crown penetrations during construction. This task is mostly carried out using methods based on triangulation (Khosravipour et al., 2016) or the fusion of morphological and graph-based approaches (Hao et al., 2019). In essence, the filtration process for an upside-down point cloud largely resembles the problem of ground point classification. In this case, one of the most widely used approaches is cloth simulation (Zhang et al., 2016) or iterative densification of TIN (Axelsson, 2000). Our workflow uses the latter approach, with calculations performed on a graphics processing unit (GPU), analogous to that described by Coll and Guerrieri (2017).

The entire tree surface filtering process was implemented as a standalone Python script. Since the full ULS point clouds used as input for the process were quite large (approximately 500 million points), it was not possible to process them all at once. To this end, the point clouds exported from GreenValley LIDAR 360 (GreenValley, 2026) software were first converted to the Cloud Optimized Point Cloud (COPC) format (Hobu Inc., 2021) using the open-source program Untwine (Hobu Inc., 2026). Next, using the octree structure stored in the COPC file, the TIN densification filtering was performed iteratively on smaller segments of the point cloud. To avoid artifacts at tile boundaries, the segments included a 10-meter buffer, ensuring consistent results. The use of a filtering algorithm removed all points below the canopy's upper surface, leaving only points on the canopy surface and the exposed ground (Figure 2). The filtering also significantly reduced the input data size, leaving only about 25% of the original points (125 out of 509 billion).

The TIN generation process was ported to C++, using the NVIDIA CUDA library. Such implementation enabled generating the filter points on the GPU, significantly reducing computation time. Since the classified points were located in the tree canopy, relatively loose criteria were applied in the filtering process. The parameters in the algorithm proposed by (Axelsson, 2000) relate to the positions of points above the TIN surface. Two of these criteria concern the angles between the point under examination and, respectively, the triangle's vertex and its edges. Due to the trees' varied shapes, these criteria were practically disregarded, with threshold values set at 80 degrees. The third criterion concerns the distance of the point under examination from the triangle's surface. To prevent the algorithm from expanding the TIN too aggressively, this value was set to 1 m.

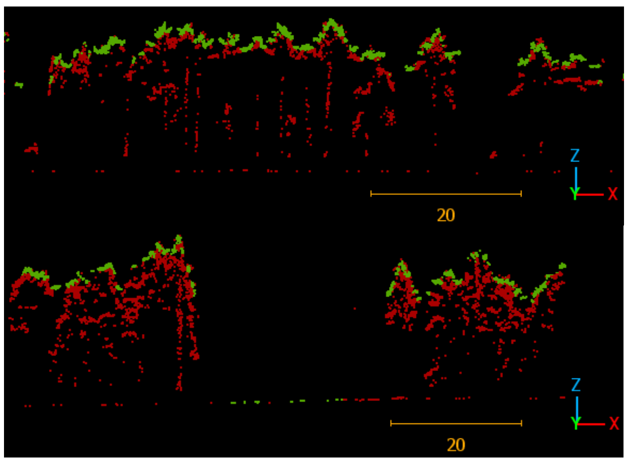

Figure 2. Examples of canopy surface filtering based on upside-down ground classification based on TIN densification. The results for the ULS data are shown. Points selected as the canopy surface are displayed in green. Points assigned below the surface are shown in red.

Because the ULS point clouds and multispectral images were acquired independently during two separate flights and because the two sensors differ in GNSS positioning accuracy, the datasets were not properly aligned. Due to the nature of the study area (dense tree cover), it was not possible to provide additional observations or GCPs to reduce geometric discrepancies between the two discussed data sources. Therefore, a new step was introduced into the data processing workflow, requiring an additional adjustment of the image data to the point cloud resulting from ULS processing. The goal of the adjustment was to align the images using a classic bundle adjustment while simultaneously aligning derived geometry to the ULS point cloud.

Consequently, a key piece of data necessary for the additional alignment was the forest canopy geometry approximation derived from MS imagery. To avoid repeatedly generating DIM products, tiepoints were used as input to the algorithm, as they sufficiently captured the forest geometry. The orientation process began with a set of images acquired using the MS camera that had already undergone preliminary orientation. This initial stage is essential for establishing spatial relationships between individual images and providing a reliable basis for further enhancement in the hybrid adjustment stage. In our case, the orientation procedure was performed using the standard image alignment and data orientation workflow implemented in Agisoft Metashape (Agisoft LLC, 2026). Upon completion of the orientation procedure, detailed information on the calculated image orientations, camera parameters, and associated control points was exported as a Blocks Exchange XML file.

For hybrid adjustment, a program was implemented that iteratively performs a nonlinear optimization, accounting for three types of observations. Two of these, known from the classical case of GNSS/INS-aided aerial triangulation, are in the form of reprojection errors at control points and GNSS positioning errors. IMU rotation errors were not included in the optimization, as the sensor used did not record them. Along with these two standard observations, an additional observation, the distances of tiepoints from the ULS point cloud, was introduced. In each iteration of the optimization process, the residuals due to reprojection error, the distance between the projection centers and the GNSS measurement, and the 3D distance between each control point and its nearest neighbor from the ULS found in that iteration are minimized. The variables optimized in this process were the parameters of extrinsic and intrinsic image orientation and sensor distortions, modeled using the standard 5-parameter Brown distortion model (3 parameters for radial and 2 for tangential distortion), and the positions of tiepoints. The algorithm's results, including newly estimated image extrinsic orientation parameters, tiepoint coordinates, and camera intrinsics, were later exported back to a BlocksExchange XML file for use in the desired photogrammetric software.

To perform the orientation described above, a new C++ tool was developed. Several open-source software libraries were used in its implementation. The most important of these include:

- PDAL - for reading and writing point clouds;
- PROJ - for converting between different coordinate systems;
- nanoflann - for constructing and querying the KD-Tree structure used to find nearest neighbors;
- Ceres Solver - for performing the optimization process.

For testing purposes, the tool was implemented as a standalone program and as Python libraries.

3. Results

3.1 Dataset

The data orientation problem concerns multispectral images and LiDAR point clouds acquired over a dense forest area (Figure 3). The data were acquired in the forestry area of the Żednia Forest District, Podlaskie Voivodeship, Poland. The data were acquired during two seasons: in April (leaf-off) and September (leaf-on) (Table 1). The area under analysis covers approximately 1.1 km^2.

The data were collected from two UAV platforms: a DJI Matrice 300 RTK equipped with a Green Valley LiAir V70 laser scanner, and a DJI Matrice 600 Pro equipped with a Micasense Dual RedEdge-MX. LiAir V70 is equipped with an IMU/GNSS receiver, and, thanks to an additional RTK base station, it is possible to post-process the trajectory using the base station's observation files. Thanks to that, the point cloud from the scanner should be highly accurate, even without using GCPs. Thus, it was used as a reference dataset in the orientation process.

Figure 3. A schematic representation of the area for which test data was collected.

	Leaf-off	Leaf-on
Number of images	5008	5089
Approximate flight altitude [m]	88.9	92.6
GSD [cm/pix]	6.2	6.4
Focal length [mm]	5.5	
Image resolution [pix]	1280 x 960	
Image overlap [%]	85 x 85	

Table 1. Key parameters related to UAV multispectal imagery

The Micasense Dual RedEdge-MX camera is not hardware-compatible with the DJI Matrice 300 RTK, meaning it does not use the UAV's RTK observations; it relies solely on its own GNSS receiver. Thus, the image positions have decimeter or even meter accuracy. After separating LiDAR and image processing, when the products generated from the data were compared, significant shifts were observed. Shifts occurred in both the vertical and horizontal axes. They were most noticeable in the tree crowns, which were displaced by nearly 2 meters in some parts of the cloud. Additionally, the shifts were not uniform across the whole area; they differed when different parts of the area were analyzed. Thus, a hybrid approach to the data was adopted.

3.2 Optimization

Before proceeding with the optimization of the MS image blocks, they were aligned in Agisoft Metashape. During alignment, the GNSS-measured camera position accuracy was set to 2 m for leaf-on data and 4 m for leaf-off data. Image tiepoint accuracy was set to 0.8 and 0.5 pixels, respectively. For the values of the deviation chosen in this way, the standard deviations for the individual types of observations were as close as possible before and after adjustment (Table 2). The same observation weights were used when optimizing the orientation of the image block relative to the ULS point clouds.

The research challenge was to determine the weights of the observations for the ICP component of the adjustment process.

Although from a mathematical standpoint, these observations play a similar role to GCPs, moderation was required when assigning their weights. Overweighting this type of observation increased the root-mean-square (RMS) reprojection error and, consequently, disrupted the internal consistency of the image block orientation. On the other hand, reducing these observations' weight too drastically prevented the point cloud from deforming. During the experiments, the effect of changing this weight on the entire leveling process was analyzed. For both blocks under analysis, the process was carried out by varying the weight from 0.1 to 1.0 m in 0.1-meter increments. During the experiments, it was observed that optimal results are obtained when the weight is set to around 0.5 m. With this observation weight, no increase in reprojection error was observed in subsequent iterations, but the displacements of tiepoints and image projection centers were available.

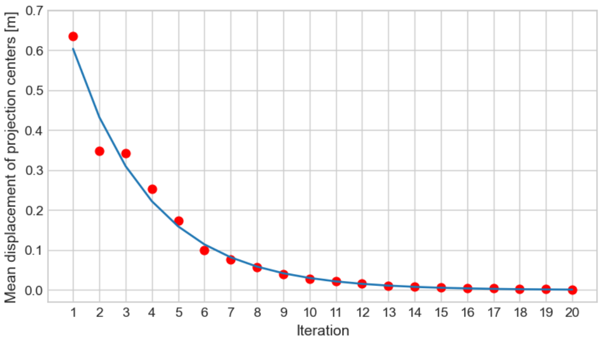

Figure 4. A graph showing the decrease in the average relative displacement of images' projection centers across successive iterations of the optimization process.

For both datasets tested, the process was run for 20 iterations. A subsequent analysis of the decline in the average displacement of the image positions between successive iterations showed that the camera positions stabilized to within a centimeter after just 10 iterations, as displayed in Figure 4.

The results of the orientation optimization for both data sources were analyzed in terms of changes in the a posteriori error of image positioning relative to GNSS measurements, as well as its relative orientation error expressed as a reprojection error relative to the assumed a priori errors (Table 2). As shown in RMS values, the reprojection error and the positional error relative to the measured GNSS positions after hybrid adjustment remain close to the a priori accuracy values used as weights. A slight increase in GNSS error is observed; however, it can be concluded that this is due to block geometry deformation.

	Rep. error [pix]	GNSS error [m]
Assumed (leaf-on)	0.800	2.00
After initial alignment (leaf-on)	0.704	1.93
After optimization (leaf-on)	0.730	2.42
Assumed (leaf-off)	0.500	4.00
After initial alignment (leaf-off)	0.579	3.87
After optimization (leaf-off)	0.577	4.13

Table 2. A comparison of the accuracy of a priori and a posteriori accuracies used in the bundle adjustment process and subsequent optimization

3.3 Synergy evaluation

Although it was not possible to create ground truth data due to the nature of the area and the datasets, a relative assessment of the algorithm's quality was conducted using two approaches: qualitative and quantitative.

A visual assessment of improvements in the image block geometry was performed by comparing the original ULS data with clouds generated by dense image matching. The comparisons were made on vertical cross-sections through the examined clouds (Figure 6) and by superimposing the DIM-derived digital surface model (DSM) and the ULS-derived canopy height model elevation models (Figure 5).

An examination of cross-sections extracted from the point clouds clearly demonstrates a substantial improvement in the relative alignment of the ULS and DIM datasets. The geometric consistency between the two datasets increases significantly, with reduced offsets visible across the compared profiles. A similar trend can be observed when analyzing digital elevation models from ULS and DIM. The visual comparison of the DSM and CHM models reveals a notably higher level of geometric consistency, reflected in the more coherent tree representation

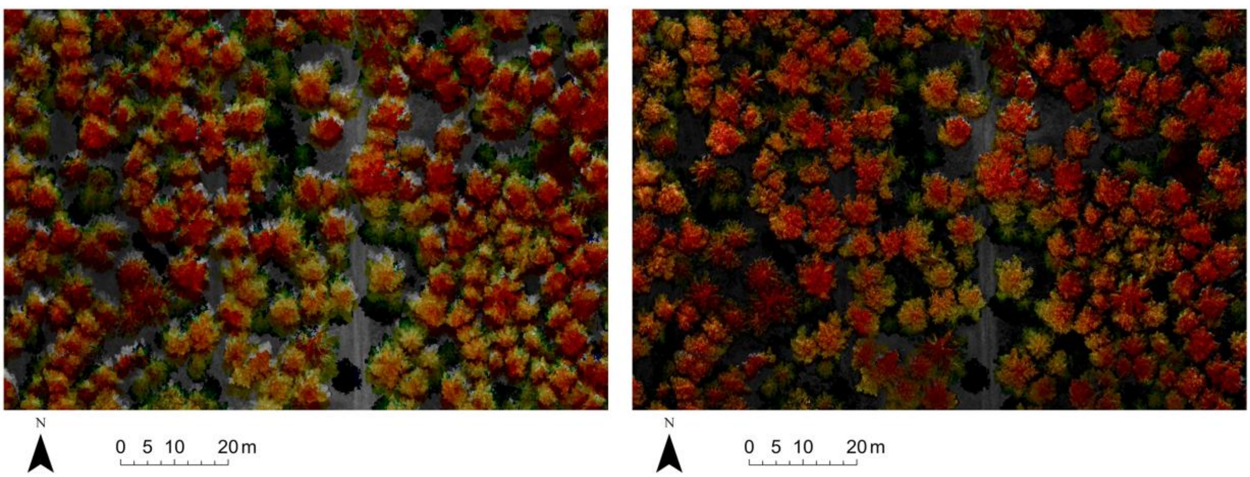

Figure 5. Comparison of the consistency of elevation models before (left) and after additional alignment (right). The green and red palette shows the CHM model created from ULS data, while the grayscale shows the DSM model from DIM.

and reduced local misalignments. These observations indicate that the applied processing steps effectively increased the spatial compatibility of both point cloud collections.

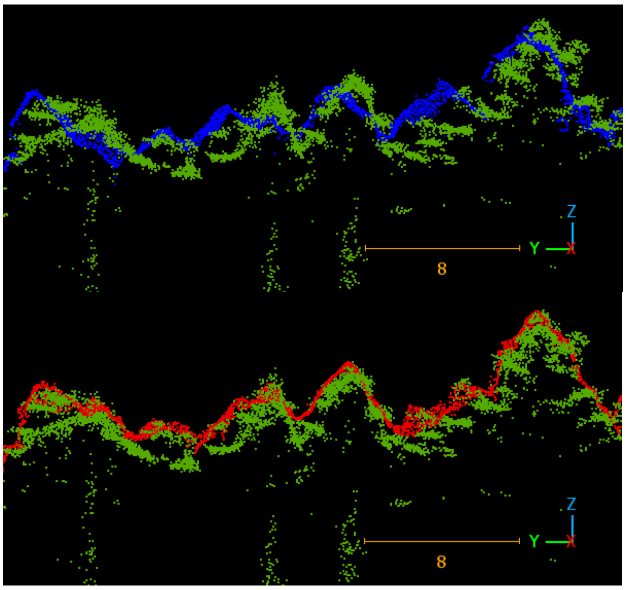

Figure 6. An example cross-section showing a point cloud from ULS (green), DIM before alignment (blue) and DIM after alignment.

To perform a quantitative assessment of the optimization quality for datasets acquired during the leaf-off and leaf-on periods, the positions of 40 tree tops, evenly distributed across the study area, were manually measured and compared using CHMs derived from ULS data, DIM data processed without the proposed algorithm, and DIM data after the application of the optimization procedure. The use of manually identified tree tops yielded a set of distinct, spatially distributed control features, enabling an objective evaluation of geometric correspondence between the datasets. The analysis focused on differences in tree top positions within the horizontal plane, allowing for the assessment of spatial alignment improvements resulting from the proposed algorithm. The obtained results demonstrate a clear enhancement in the relative alignment between DIM-derived and ULS-derived datasets after optimization:

- In the case of leaf-off data, a substantial decrease in the average position error relative to ULS data was observed. The average horizontal position error relative to the ULS reference data decreased from 1.25 m to 0.60 m, corresponding to an improvement of more than 50%. Similarly, the largest recorded positional difference was reduced from 1.92 m to 1.04 m;
- Comparable improvements were identified for the leaf-on dataset. The mean horizontal error decreased from 0.96 m to 0.45 m, while the maximum offset between the tops of the analyzed trees was reduced from 1.79 m to 0.70 m. The lower residual errors observed after optimization demonstrate that the algorithm was equally effective under leaf-on conditions, despite the increased complexity associated with denser vegetation and potentially more challenging image matching conditions.

Particular attention should be given to the differences in both the magnitude and direction of deformation observed between the image blocks and the ULS reference data. These deformation patterns, illustrated in Figure 7, reveal that the discrepancies are not spatially uniform but exhibit an irregular, locally variable character. The results demonstrate that applying the proposed workflow significantly reduced these irregular deformations and improved overall geometric agreement between the MS and ULS datasets. Following the optimization process, the magnitude of local discrepancies decreased, and the directional inconsistency of offsets became noticeably less pronounced. This indicates that the proposed approach effectively addressed both systematic and locally varying geometric distortions, leading to a more spatially coherent integration of the datasets.

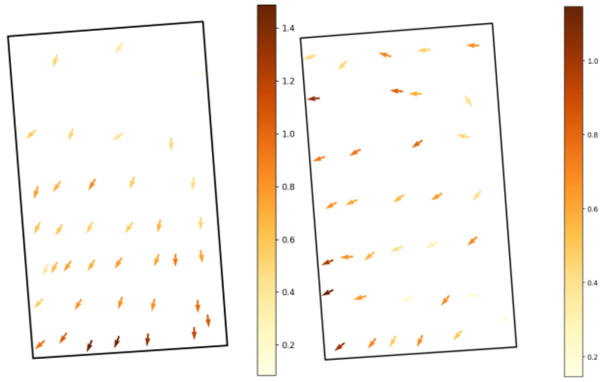

Figure 7. Visualization of the direction and magnitude of deformation of the image block during the optimization process, determined based on measured tree tops. The image on the left shows the results for leaf-off data, and the image on the right shows the results for leaf-on data. The direction of the arrow indicates the direction of deformation, and the color scale represents the length of the tree-top displacement vector.

4. Conclusions

This research demonstrates that combining bundle adjustment with an ICP-based alignment step provides an effective solution for improving the geometric consistency between multispectral image blocks and ULS point clouds acquired in dense forest environments.

The proposed workflow addresses a key limitation of traditional orientation methods, which rely heavily on GCPs - often unavailable, unreliable, or impractical to obtain under dense canopy conditions. By incorporating canopy-level correspondences and a joint optimization strategy, the method successfully mitigates systematic discrepancies arising from independent GNSS/IMU errors for both sensors.

The results obtained for both leaf-off and leaf-on datasets clearly confirm the effectiveness of the combined adjustment. After applying the proposed method, the average horizontal offset between DIM-derived treetops and ULS-derived treetops was reduced by more than 50% in both seasonal scenarios. The maximum discrepancy also decreased substantially, demonstrating that the hybrid approach improves not only the overall block geometry but also the local accuracy across the study area. Visual inspection of DSM–CHM overlays and cross-sections further supports this improvement, showing significantly enhanced surface coherence after adjustment.

The introduced workflow, comprising GPU-accelerated canopy filtering and a customized bundle adjustment with ICP constraints, is a robust and flexible tool for fusing heterogeneous datasets in forested regions. Its ability to operate without GCP makes it particularly valuable for UAV-based forestry applications, where obtaining high-quality ground references is often challenging.

Future work will focus on testing the proposed algorithm using a broader range of datasets acquired under different environmental and topographic conditions. Particular attention will be given to areas characterized by simpler terrain geometry, where geometric distortions may be less pronounced. In such cases, the objective will extend beyond improving dataset alignment to investigate the potential to reduce or eliminate the need for field GCP measurements. This direction may simplify data acquisition workflows and increase the operational efficiency of photogrammetric processing while maintaining satisfactory geometric accuracy.

References

Agisoft LLC, 2026. Agisoft Metashape. agisoft.com (18 May 2026)

Axelsson, P.E., 2000. DEM generation from laser scanner data using adaptive TIN models. *International Archives of the Photogrammetry and Remote Sensing, 33, 110-117.*

Clédat, E., Skaloud, J., 2020: Fusion of photo with airborne laser scanning. *ISPRS Annals of the Photogrammetry, Remote Sensing and Spatial Information Sciences, 1, 173-180.*

Coll, N., Guerrieri, M., 2017: Parallel constrained Delaunay triangulation on the GPU, *International Journal of Geographical Information Science, 31:7, 1467-1484*, DOI: 10.1080/13658816.2017.1300804

Glira, P., Pfeifer, N., Mandlburger, G., 2019. Hybrid orientation of airborne LiDAR point clouds and aerial images. *ISPRS Annals of Photogrammetry, Remote Sensing and Spatial Information Sciences, Geospatial Week 2019, Enschede, NL*

GreenValley, 2026. LiDAR 360. greenvalleyintl.com/LiDAR360 (18 May 2026).

Haala, N., Kölle, M., Cramer, M., Laupheimer, D., Mandlburger, G., Glira, P., 2020. Hybrid georeferencing, enhancement and classification of ultra-high resolution UAV LiDAR and image point clouds for monitoring applications. *ISPRS Annals of Photogrammetry, Remote Sensing and Spatial Information Sciences*, *V-2-2020, 727–734*

Hao, Y., Zhen, Z., Li, F., Zhao, Y., 2019. A graph-based progressive morphological filtering (GPMF) method for generating canopy height models using ALS data. *International Journal of Applied Earth Observation and Geoinformation*, *79*, 84-96.

Hobu Inc., 2021. Cloud Optimized Point Cloud Specification. copc.io (18 May 2025)

Hobu Inc., 2026. Untwine. github.com/hobuinc/untwine (18 May 2026)

Khosravipour, A., Skidmore, A. K., Isenburg, M., 2016. Generating spike-free digital surface models using LiDAR raw point clouds: A new approach for forestry applications. *International journal of applied earth observation and geoinformation*, *52*, 104-114.

You, H., Tang, X., You, Q., Liu, Y., Chen, J., Wang, F., 2023. Study on the Differences between the Extraction Results of the Structural Parameters of Individual Trees for Different Tree Species Based on UAV LiDAR and High-Resolution RGB Images. *Drones*, *7*(5), 317. DOI: 10.3390/drones7050317

Zhang, W., Qi, J., Wan, P., Wang, H., Xie, D., Wang, X., Yan, G., 2016. An Easy-to-Use Airborne LiDAR Data Filtering Method Based on Cloth Simulation. *Remote Sensing. 2016; 8(6):501*.

Zhou, T., Hasheminasab, S. M., Habib, A., 2021. Tightly-coupled camera/LiDAR integration for point cloud generation from GNSS/INS-assisted UAV mapping systems. *ISPRS Journal of Photogrammetry and Remote Sensing*, *180*, 336-356.